

Computer simulation of short-range repulsion between supported phospholipid membranes

Alexander Pertsin, Dmitry Platonov, and Michael Grunze^{a)}

Angewandte Physikalische Chemie, Universität Heidelberg, Im Neuenheimer Feld 253, 69120 Heidelberg, Germany

(Received 6 February 2006; accepted 6 March 2006; published 14 April 2006)

The grand canonical Monte Carlo technique is used to calculate the water-mediated pressure between two supported 1,2-dilauroyl-DL-phosphatidylethanolamine (DLPE) membranes in the short separation range. The intra- and intermolecular interactions in the system are described with a combination of a united-atom AMBER-based force field for DLPE and a TIP4P model for water. The total pressure is analyzed in terms of its hydration component and the component due to the direct interaction between the membranes. The latter is, in addition, partitioned into the electrostatic, dispersion, and steric repulsion contributions to give an idea of their relative significance in the water-mediated intermembrane interaction. It is found that the force field used exaggerates the water affinity of the membranes, resulting in an overestimated hydration level and intermembrane pressure. The simulations of the hydrated membranes with damped water-lipid interaction potentials show that both the hydration and pressure are extremely sensitive to the strength of the water-lipid interactions. Moreover, the damping of the mixed interactions by only 10%–20% changes significantly the relative contribution of the individual pressure components to the intermembrane repulsion. © 2006 American Vacuum Society. [DOI: 10.1116/1.2190699]

I. INTRODUCTION

The short-range repulsive force occurring between phospholipid membranes in water and aqueous solutions has long been of interest to physicists and biologists, mainly in the context of cell recognition, adhesion, and fusion.¹ Despite considerable progress in direct experimental measurements of intermembrane forces using the surface force apparatus (SFA) and atomic force microscopy, the nature of the short-range repulsion is still poorly understood.² In a general case, the instantaneous force operating between two parallel membranes, m and m' , across the water gap can be represented as the sum of the force exerted on membrane m by water molecules, $f_{w \rightarrow m}$, and the force due to direct interaction between the membranes $f_{m' \rightarrow m}$. Such a representation is correct inasmuch as the three- and higher-body effects in the intermolecular interaction energy can be neglected. The ensemble average of the water-membrane force, $\langle f_{w \rightarrow m} \rangle$, defines the hydration (solvation) pressure, $p_h = A^{-1} \langle f_{w \rightarrow m} \rangle - p_b$,³ where A is the membrane area and p_b is the bulk water pressure. Adding the pressure component arising from the direct intermembrane interaction, $p_d = A^{-1} \langle f_{m' \rightarrow m} \rangle$, one gets the net pressure, $p = p_h + p_d$, as measured in a SFA experiment. To avoid misunderstanding, it is worth noting that the term “hydration pressure” or, more generally, “solvation pressure” is frequently used to mean the net pressure p and not p_h . Here we prefer to follow the terminology of Evans and Marconi,³ wherein p_h refers to the *genuine* solvation pressure, free from the direct interaction between the surfaces that confine the solvent.

The origin of short-range intermembrane repulsion was initially associated with the hydration pressure p_h .^{4–6} Considering the high hydrophilicity of the membrane surface, the repulsion was ascribed to the energy loss due to the exclusion of water and the associated dehydration of the membranes when they approached each other. The hydration repulsion had also a “structural” interpretation, which involved orientational polarization or “structuring” of water next to the membrane surface. The weaknesses involved in the hydration mechanism of the short-range repulsion were discussed at length by Israelachvili and Wennerström.^{2,7} It was argued, in particular, that the range of orientational polarization in water was limited by one or two water diameters, which was noticeably less than the observed range of the hydration force. This argument is particularly true of phospholipid membranes, where the range of orientational polarization is restricted by a high molecular-level roughness of the membrane surface.

The alternative explanation suggested by Israelachvili and Wennerström^{2,7} for the short-range repulsion implies the dominant role of direct intermembrane interactions, as characterized by p_d . In this explanation, the repulsion arises from entropy-driven deviations of hydrated membranes from ideal planar geometry. Most important deviations are thermal undulations of the membrane surface, fluctuations in the membrane thickness (like peristalsis), and protrusion of individual lipid molecules and/or their headgroups into the aqueous phase. The deviations of this kind are taken into account by adding appropriate correction terms to the force calculated on the assumption of the ideal membrane geometry. Following Israelachvili and Wennerström,^{2,7} these correction terms are usually referred to as the undulation, peristaltic, and protrusion forces or, together, the entropic forces. For mem-

^{a)}Electronic mail: michael.grunze@urz.uni-heidelberg.de

branes supported on flat rigid substrates (as studied in SFA experiments), the only significant force of this kind is the protrusion force. Note that the protrusion force is not a new physical type of force. It enters into p_d provided that the ensemble averaging properly samples protruded configurations.

The weaknesses of the Israelachvili and Wennerström's^{2,7} ideas have been discussed by Parsegian and Rand.⁸ It was in particular noted that the suggested dependence of the protrusion energy on the molecular out-of-plane displacement would lead to impossibly high solubilities of phospholipids in water. It was also argued that the protrusion force could not explain the observed strong effect of a single methylation of an ethanolamine group on the intermembrane force: Would the repulsion be due to molecular protrusions, it would not be so sensitive to the methylation of the headgroup.

Unfortunately, the theoretical treatments of both the hydration and entropic forces involve serious simplifications and a number of unknown parameters. The improvement and verification of theory are only possible on the basis of a molecular-level knowledge of the membrane structure along with the simultaneous knowledge of the water-mediated intermembrane force. This attaches significance to direct computer simulations of the force as the respective ensemble average. An advantage of computer simulation is the possibility to partition the calculated net force into physically distinct components associated with the individual components of the potential energy. Furthermore, the direct intermembrane pressure p_d can be decomposed into contributions from individual lipid molecules, which allows, in particular, an analysis of molecular protrusions and their contribution to the short-range repulsion.

An attempt at direct computer simulation of the operative force between phospholipid membranes in water has been undertaken in our recent work⁹ using the grand canonical Monte Carlo (GCMC) technique. The configuration of the model system was similar to that of a SFA experiment (Fig. 1): Two 1,2-dilauroyl-DL-phosphatidylethanolamine (DLPE) membranes were supported on parallel solid substrates and brought to equilibrium with bulk water at ambient conditions. The starting membrane structure was constructed based on the x-ray diffraction data for the DLPE-acetic acid crystal.¹⁰ During the simulations, the area per DLPE molecule was kept fixed at the respective crystal-state value, $A=38.6 \text{ \AA}^2$. The net intermembrane pressure p was analyzed in terms of p_h and p_d . The latter was, in addition, partitioned into the electrostatic, dispersion, and steric repulsion components, hereafter p_d^{elst} , p_d^{disp} , and p_d^{rep} , respectively. The simulation showed that none of the pressure components could be neglected at short separations. Among these non-negligible components was p_d^{elst} originating from direct electrostatic interaction between the lipid headgroups in the opposite membranes. Due to the high packing density of the membranes, the out-of-plane motion of the lipid molecules was restricted. In addition, the force field used involved a defect which forced the ethanolamine group to assume an unlikely *cis* con-

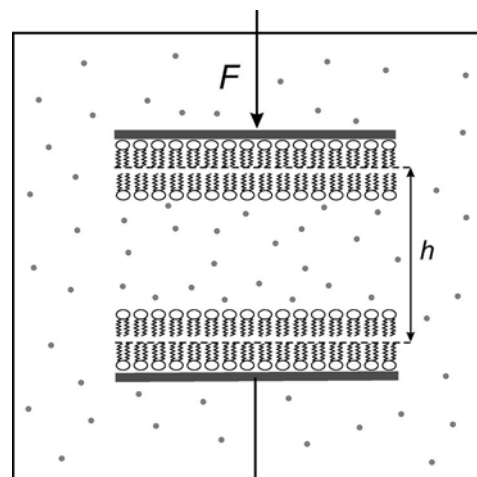


FIG. 1. Configuration of a SFA experiment with lipid membranes. The dashed lines show the position of generalized substrates when the outer monolayers are treated implicitly.

formation about the C–C bond. All this suppressed molecular and headgroup protrusions, so that no perceptible manifestation of the protrusion force could be detected.

In the present study, we extend our GCMC simulations to a substantially larger area per molecule, $A=51.2 \text{ \AA}^2$, as observed experimentally for the fluid-phase DLPE at 308 K.^{11,12} The simulations are carried out at three selected substrate-to-substrate separations corresponding to repulsive pressures on the order of 1 kbar (10^9 dyn cm^{-1}). The distribution of the water-mediated pressure over its major components is analyzed against the water-induced changes in the membrane structure. A few comparative simulations are also made for the phosphatidylcholine (PC) analog of DLPE, DLPC.

II. METHOD

Although the ensemble averages $\langle f_{w \rightarrow m} \rangle$ and $\langle f_{m' \rightarrow m} \rangle$ needed to evaluate the intermembrane pressure can in principle be calculated by molecular dynamics (MD)—the predominant method used in studies of lipid membranes—we preferred to resort to the GCMC technique. This choice is motivated by, at least, two reasons. First, GCMC is best suited for simulating a SFA experiment, where confined water is allowed to exchange molecules and is in the chemical equilibrium with a bulk water reservoir (Fig. 1). Unlike MD simulations, where the number of water molecules per lipid, n_w , is kept fixed at the respective experimental value, GCMC does not need the knowledge of n_w and treats it as a variable which adjusts itself so as to equilibrate confined water with bulk water. Second, with a judicious choice of the sampling procedure and parameters, GCMC is more efficient in exploring the configurational space of the hydrated membrane. Unlike MD, GCMC is not tied to the time evolution of the system, and so it can efficiently explore the membrane's configurational space using various “unphysical” moves. This is particularly important in simulations of hydrated lipid membranes where an adequate description of the permeation of

water in the membrane may involve difficulties. The difficulties can be appreciated from an estimate of the number of water molecules that cross the membrane in the accessible time scale of MD simulations.^{13,14} For a typical length of the MD trajectory (1–10 ns) and a typical area of the membrane repeat unit ($\sim 1000 \text{ \AA}^2$), this number proves to be as small as 0.01–0.1. That is the probability of a water molecule finding its way to the membrane interior by normal diffusion is extremely low. By contrast, in a GCMC simulation, the water molecule need not diffuse through the whole monolayer thickness to reach the middle of the membrane. It can well do this by an unphysical particle insertion move. The stimulating role of unphysical moves in equilibrating the distribution of water through the membrane has been demonstrated by Jedlovsky and Mezei,¹⁴ who compared water density profiles calculated by GCMC and a standard *NVT* ensemble Monte Carlo. (Note that the latter is similar to MD in the respect that in both cases water molecules may penetrate into the membrane only by diffusion.) In similar conditions, GCMC showed a substantially deeper water penetration and an order of magnitude faster convergence to equilibrium.

A. Force field

Because of a high computational cost of GCMC simulations, where most of attempted configurations are spent for unsuccessful insertions, our choice of the inter- and intramolecular potential functions was restricted to computationally less demanding force fields of the united-atom type. As in our simulations at the crystal-state DLPE density,⁹ the conformational and intermolecular energies of DLPE molecules were calculated using an AMBER-based force field, whose torsional parameters were refined by Smondyrev and Berkowitz¹⁵ based on *ab initio* energy profiles and equilibrium geometries of eight compounds modeling individual fragments of dipalmitoylphosphatidylcholine (DPPC). For the ethanolamine group, which is absent in DPPC, we initially used the relevant potentials from the GROMACS force field.¹⁶ Although the latter is a united-atom force field, it treats the hydrogen atoms of the amino group explicitly. Each hydrogen atom bears a partial charge but no Lennard-Jones force center. The interactions of water molecules between themselves were described with the four-site TIP4P model.¹⁷

Trial simulations of hydrated DLPE membranes showed however that the earlier-described force field led to an unrealistic distribution of the O–C–C–N dihedral angles in the ethanolamine group, such that the most preferred conformer about the C–C bond was *cis*. To make sure that this result was not due to the interaction of the ethanolamine group with water, we carried out simulations of an anhydrous crystal-like DLPE bilayer. The most preferred conformer proved again to be *cis*, which was at variance with the available x-ray diffraction data for crystalline phospholipids,¹⁸ which favored a *gauche* conformer. An analysis of the simulated DLPE conformations showed that the *cis* conformer was stabilized by a strong N–H \cdots O hydrogen bond, which formed between the ethanolamine oxygen and nitrogen at-

oms and whose formation led to large deformations of the bond angles in this group. In an attempt to avoid this hydrogen bond, we unsuccessfully tried the torsion O–C–C–N potential suggested by Smondyrev and Berkowitz¹⁵ for choline and claimed to be suitable for ethanolamine as well. Also unsuccessful was our attempt to solve the problem by placing Lennard-Jones force sites on the amine hydrogen atoms, as in the all-atom version of the AMBER force field.¹⁹ In the end, the undesirable hydrogen bonding was avoided by a twofold attenuation of the (1–5) Coulombic interaction H \cdots O in the ethanolamine group.

In an attempt to improve the balance of the water-lipid, water-water, and lipid-lipid interactions, we also tried to damp the water-lipid interactions by multiplying the relevant contributions to the instantaneous potential energy and force by a factor $\alpha < 1$. The incentive to this part of our study will be clear from the discussion of the simulation results in the next section. In calculations of the potential energy of the DLPE-water system, the long-range contribution to the electrostatic energy was treated in the group-based dipole-dipole approximation. The DLPE molecule was represented as a set of electrically neutral groups as described by Smondyrev and Berkowitz.¹⁵ The reliability of the dipole-dipole approximation for long-range electrostatic interactions in DLPE membranes has been demonstrated elsewhere.⁹ Quite an acceptable accuracy of 0.3% for the electrostatic energy was achieved when the truncation radii for charge-charge and dipole-dipole interactions were taken to be 20 and 100 \AA , respectively. Such an accuracy is noticeably worse than that reported for the particle mesh Ewald method usually used in MD simulations.²⁰ It hardly makes sense, however, to strive for a better accuracy because the very representation of the molecular (continuous) charge distribution in terms of partial atomic charges introduces a much larger error in the electrostatic interaction energy.

As in our previous work,⁹ only the two inner DLPE monolayers were treated explicitly, whereas the outer monolayers were considered as generalized substrates for the inner ones (Fig. 1). The associated substrate potential described, in a mean-field manner, the interaction between the adjacent inner and outer DLPE monolayers. It was parametrized so as to fit atomistic force field results for the interaction energy of two DLPE monolayers facing each other with their hydrophobic sides. The parametrization was made in the following way. We first calculated the non-bonded energy, $U(z)$, of a perfect crystal-state DLPE bilayer as a function of the separation z between its constituent monolayers. The separation was defined as the spacing between the planes passing through the γ -chain methyl carbons in each monolayer. To bring the area per molecule to the fluid-phase value of 51.2 \AA^2 , the bilayer lattice periods were stretched by a factor of $(51.2/38.6)^{1/2} = 1.152$. The monolayer-monolayer interaction energy was calculated using the above-mentioned AMBER-based force field.¹⁵ The position of the minimum of $U(z)$, z_m , proved to be close to zero separation ($z_m = 0.15 \text{ \AA}$); i.e., in the minimum energy configuration the γ -chain methyl carbons of the two monolayers lay nearly in

TABLE I. Parameters of the atom-substrate potentials in Eq. (1).

Atom	n	m	$C_n \times 10^{-3}$ (kcal mole $^{-1}$ Å n)	C_m (kcal mole $^{-1}$ Å m)	z_0 (Å)
Methylene carbon	10	4	1211	740	-3.64
Methyl carbon	10	4	1476	900	-3.64

the same plane, in agreement with the experimental crystal structure ($z=0.08$ Å).¹⁰ For the potential well depth, we found $\varepsilon=-U(z_m)=4.8$ kcal mole $^{-1}$. The calculated dependence $U(z)$ was then fitted by the sum of atom-substrate potential functions so as to exactly reproduce z_m and ε and also to get the best agreement for the curvature of $U(z)$ at the minimum. The monolayer-substrate potential was of the form

$$\Phi = \sum_i [C_n(z_i - z_0)^{-n} - C_m(z_i - z_0)^{-m}](n > m), \quad (1)$$

where the summation is over the carbon atoms of the hydrocarbon tails of the inner monolayer; m , n , C_n , C_m , and z_0 are the potential parameters to be found; z_i is the separation of atom i from the generalized substrate placed at the plane of the γ -chain methyl carbons of the outer monolayer. The final parameter set is presented in Table I.

It should be noted that in our previous simulations⁹ the substrate-monolayer interactions were described by another model potential, with $z_m=3.5$ Å. The advantage of the present choice, with the minimum of Φ close to the crystal-state bilayer center, is that the substrate-to-substrate separation h is now closer to the lamellar repeat period, D , as measured by diffraction methods in multilamellar lipid dispersions. For the perfect crystal-state bilayers used in parametrization of Φ , the bilayer center is located at a distance of $z_m/2$ from the substrate, so that $h-D=2 \times z_m/2=0.15$ Å. For the gel and fluid states, the difference between D and h does not seem to be greater than 1–1.5 Å. Thus, in a MD simulation of the gel-phase DPPC, Venable *et al.*²¹ found that the average position of the γ -chain methyl carbons was 0.6 Å from the bilayer center. Would the generalized substrate model with parameters from Table I reproduce exactly the same density distribution, the substrate position would be ~ 0.15 Å from the average position of the γ -chain methyl carbons, so that the difference between D and h would be $2 \times (0.6 - 0.15) = 0.9$ Å. In actual fact, the difference may be somewhat larger because of inaccuracies involved in the mean-field treatment of the outer monolayers. For fluid-phase DPPC, the MD result for the average deviation of the methyl carbons from the bilayer center is 2.06 ± 2.4 Å (with no distinction between the β and γ chains). Considering that the γ chain is, on the average, closer to the bilayer center by about one C–C bond length (~ 1.5 Å),²² the average position of the γ -chain methyl carbons relative to the bilayer center, as well as the difference between D and h , should not differ significantly from those for the gel phase.

B. Starting configurations

The starting configurations of the system were constructed on the basis of the structure of DLPE monolayers observed experimentally in the DLPE-acetic acid crystal. The simulation cell contained a total of 64 lipid molecules (32 molecules per monolayer or 4×4 monolayer unit cells). The monolayers were placed with their hydrophobic sides on two parallel (generalized) substrates spaced a distance h . The initial separation of the terminal carbon atoms of from the respective generalized substrates was set at 0.15 Å, i.e., at the equilibrium distance of the monolayer-substrate potential $\Phi(z)$. The gap between the monolayers was first filled with water molecules at random positions and orientations, with the only constraint that the distance between two water oxygens and between a water oxygen and a DLPE atom was not less than 2.9 Å. After that a low temperature ($T=5$ K) *NVT*-ensemble Monte Carlo run was carried out to allow the system to assume an energetically favorable configuration. It is this configuration which was used in GCMC simulations as the starting one.

C. Simulation protocols

In our GCMC simulations only the number of water molecules was allowed to fluctuate, while the number of lipid molecules was fixed, i.e., the system was actually treated in a semigrand canonical ensemble.²³ To improve the efficiency of water insertions, the excluded volume mapping,²⁴ closely related to the Mezei's cavity-bias technique,²⁵ was employed, with the shortest allowed water-water separation of 2.4 Å. Further improvement in sampling efficiency was achieved using a Swendsen-Wang filtering.²⁶ The filtering out of energetically unfavorable insertions and deletions was based on a computationally inexpensive energy predictor, in which the electrostatic contribution to the water-water and water-lipid interactions was omitted. The frequencies of attempting water insertions and deletions were taken to be in the ratio 10:1.

A displacement move of a water molecule was made by translating its center of mass by a random vector and then rotating the molecule by a random angle about one of the three space-fixed axes chosen at random. A move of a DLPE molecule was defined to include a conformational change and a positional displacement of the molecule as a whole. The changes in the molecular conformation of DLPE were made subject to bond-length constraints, based on a rotational displacement algorithm suggested in our early work.²⁷ A single conformational change affected all torsion and bond angles in the lipid molecule. The moves of water molecules were attempted at a ten times higher rate than the moves of lipid molecules.

The chemical potential of confined water was specified by setting the "density-corrected" excess chemical potential $\mu'' = \mu' + kT \ln d$,²⁸ where μ' is the excess (configurational) chemical potential²⁹ and d is the average water density in grams per cubic centimeter. For bulk liquid water, d is close to unity and μ'' is practically equal to μ' . The value of μ''

TABLE II. Hydration degree and water-mediated pressure (kbar) as a function of substrate-to-substrate separation h and damping factor α .

$h, \text{\AA}$	α	n_w	p	p_h	p_d	p_d^{elst}	p_d^{disp}	p_d^{rep}
42.6	1.0	11.0	5.0	4.1	0.9	0	-2.1	3.0
44.1	1.0	11.7	4.4	2.0	2.4	3.0	-0.7	0.1
	0.9	9.8	1.6	2.1	-0.5	-1.5	-2.0	3.0
	0.8	8.5	0.5	1.4	-0.9	-1.5	-1.8	2.4
	0.7	6.3	-0.8	1.4	-2.2	-6.7	-3.6	8.1
45.6	1.0	13.1	3.7	1.4	2.3	2.0	-0.6	0.9

was set at $-5.95 \text{ kcal mole}^{-1}$, as determined in separate simulations of bulk TIP4P water so as to reproduce best the experimental density of water at $T=308 \text{ K}$. The three selected separations used in our simulations were $h=42.6$, 44.1 , and 45.6 \AA . For each particular h tried, a series of sequential GCMC runs was carried out until the difference in $\langle N \rangle$ between consecutive runs was within 3–5 particles. The length of an individual run was 1.5×10^6 GCMC passes, each comprising N_0 moves, where N_0 is the initial number of water molecules in a given pass. The total number of configurations attempted at a given h amounted to 10^{10} .

III. RESULTS AND DISCUSSION

A. Force-distance dependence

We began our simulations with $h=44.1 \text{ \AA}$, well below the experimental value of D at zero (atmospheric) pressure, i.e., at full hydration ($D^0=46.1 \pm 0.3 \text{ \AA}$).^{11,30} The starting number of water molecules generated at random as described in the previous section was 180, which corresponded to $n_w=2.8$. After a series of eight GCMC runs, n_w stabilized at 11.7 (Table II, the results for $\alpha=1$). From the atomic density profiles along the normal to the substrate plane (Fig. 2), one can appreciate a deep penetration of water in the membranes, such that a perceptible water density occurs even in the hydrocarbon region. Several water molecules attained the hy-

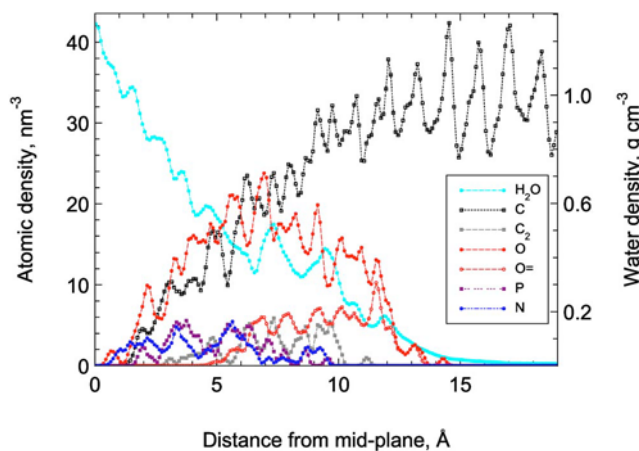


FIG. 2. Atomic density profiles in hydrated DLPE membranes at $h=44.1 \text{ \AA}$. To improve statistics, the profiles are symmetrized (e.g., averaged over the two symmetrically equivalent parts of the system).

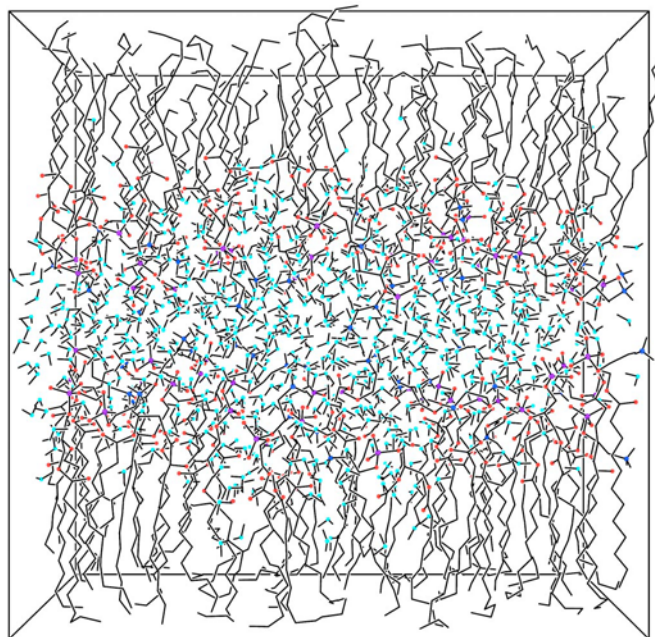


FIG. 3. Snapshot of a typical configuration of the DLPE-water system at $h=44.1 \text{ \AA}$. The DLPEs O, N, and P atoms are shown as red, blue, and purple spheres, respectively, whereas the water O atoms are represented by turquoise spheres. The carbon and hydrogen atoms are not shown.

drocarbon tails can also be observed in Fig. 3, which presents a snapshot of a typical configuration of the equilibrated system. In the context of the discussion of molecular protrusions, the positional disorder of the DLPE molecules along the z axis should be noted. This kind of disorder is well seen from the density profile of the C_2 atoms (Fig. 2), which are the topological centers of the DLPE molecules. The extent of positional disorder can be quantified in terms of the width of the C_2 density profile, which is as large as 8.6 \AA . That is, the protrusions of the individual lipid molecules from the average level into the aqueous phase may roughly be up to 4.3 \AA , i.e., more than three CH_2 units.

As the system approached equilibrium and the number of water molecules increased, the phosphatidylethanolamine (PE) headgroup backbone, $(C_2-C_1)-O_{11}-P-O_{12}-C_{11}-C_{12}-N$,³¹ experienced substantial conformational changes. In the initial (crystal) state, the conformations about the bonds $O_{11}-P$, $P-O_{12}$, and $C_{11}-C_{12}$ are fairly close to *gauche* (to within 10°), whereas the torsion angle describing rotation about the $O_{12}-C_{11}$ bond is 106° . As a consequence, the headgroup has a convoluted conformation, such that the $N \cdots C_2$ distance is 6.5 \AA . With increasing N , the conformational distribution of the headgroups exhibited more extended conformations due to the appearance of additional, *trans* conformers about the bonds of the headgroup backbone. The extension of the headgroups is illustrated in Fig. 4 (data for $\alpha=1$), which depicts the ensemble averaged distribution of the $N \cdots C_2$ distances in the equilibrated system. The obvious driving force behind the unfolding of the strongly hydrophilic headgroup is the tendency to make its potential hydrogen bonding sites more accessible to water

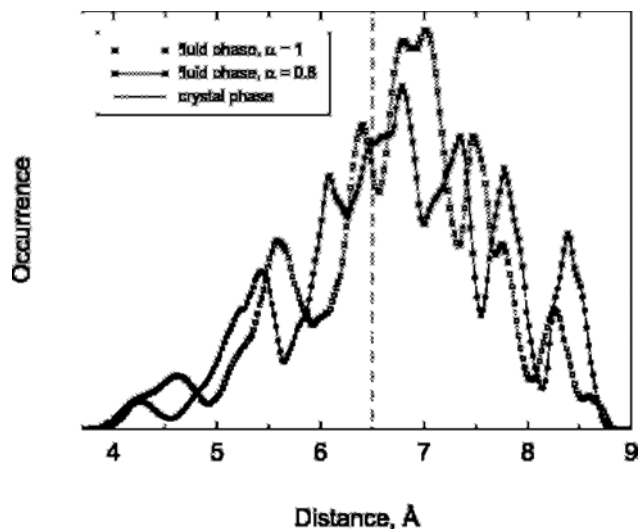


FIG. 4. Distribution of the $N \cdots C_2$ distance in hydrated DLPE membranes and DLPE-acetic acid crystal (see Ref. 10).

molecules. Aside from becoming longer, some headgroups assumed orientations close to the normal to the membrane plane, \mathbf{n} , directed towards the opposing membrane. This was well seen from an increase in the orientation parameter $S_{0.8}^{PN}$ which characterized the proportion of such orientations in terms of the cosine distribution of angles θ_i formed by PN vectors with the respective normal \mathbf{n} . More precisely, $S_{0.8}^{PN}$ was defined as the average probability density of $\cos(\theta_i)$ in the range $\cos(\theta_i) > 0.8$ ($\theta_i < 37^\circ$). The net result of the unfolding and reorientation of headgroups was the appearance of headgroups protruded into the aqueous phase. These headgroups can well be seen in Fig. 5, which shows the same

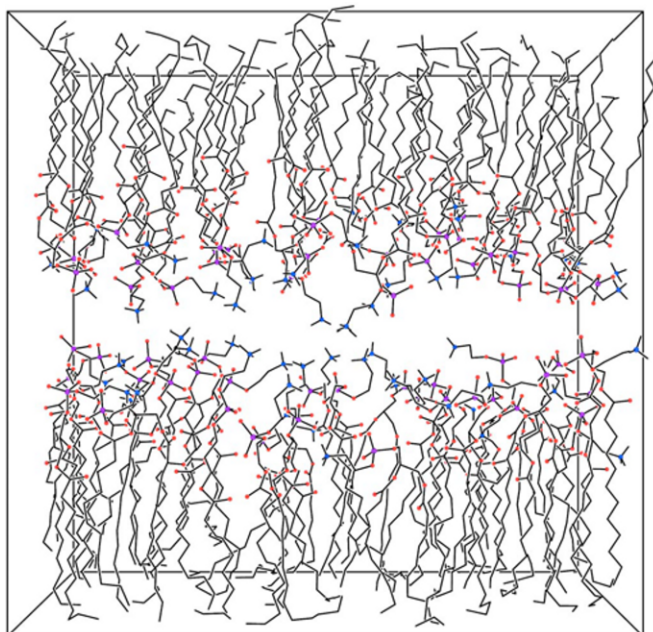


FIG. 5. Same as in Fig. 3 but without water molecules.

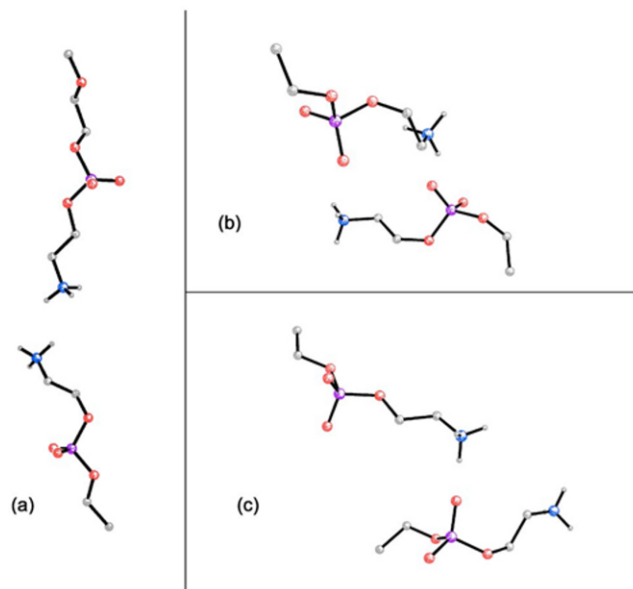


FIG. 6. Typical pairs of opposing PE headgroups characterized by strong electrostatic repulsion (a) and attraction (b), (c).

configuration as in Fig. 3, except that the water molecules are not shown for clarity.

As seen from Table II, at $h=44.1$ Å the membranes experience a strong repulsion. A large part of this repulsion originates from the hydration pressure p_h . However, the dominant contribution is due to the direct electrostatic interaction between the membranes, as described by p_d^{elst} . Moreover, nearly all p_d^{elst} comes from its static part, $p_d^{\text{elst},0}=2.9$ kbar. An analysis of the contribution of individual lipid pairs to $p_d^{\text{elst},0}$ in the final configuration of the system shows that the repulsion arises mainly from the molecules whose headgroups are protruded towards each other from the opposite membranes. A pair of such molecules, which affords about 6% of $p_d^{\text{elst},0}$, is shown in Fig. 6(a). Although the interaction energy of these molecules is positive (~ 14 kcal mole $^{-1}$), it is negligibly small compared to the variable part of the total potential energy of the hydrated membranes (-2.6×10^5 kcal mole $^{-1}$). That is why the occurrence of such molecular configurations is not improbable. It is important to note that the upper of the molecules depicted in Fig. 6(a) showed the largest out-of-plane displacement in the final configuration of the system (~ 3.8 Å). At the same time, a significant repulsive contribution to $p_d^{\text{elst},0}$ (5%–6%) was also observed for molecular pairs whose constituent molecules showed only slight out-of-plane displacements. This suggests that the protrusions of lipid molecules as a whole do not play a decisive role in the short-range repulsion. The repulsion originates from the water-induced unfolding and reorientation of headgroups, leading to the appearance of repulsive configurations such as the one depicted in Fig. 6(a).

The increase of the substrate-to-substrate separation to 45.6 Å led, as expected, to a drop in the water-mediated pressure, mainly at the expense of a decrease in its hydration component (Table II). The electrostatic repulsion between protruded headgroups remained the dominant contribution to

the total pressure. Quite a different situation was observed at the shortest separation tried, $h=42.6$ Å. Because of the closer approach of the membranes to each other, it became possible for the opposing headgroups to assume energetically favorable configurations like the ones shown in Figs. 6(b) and 6(c). In configuration (b), the positively charged ammonium groups are located opposite the negatively charged phosphate groups, which results in a strong attractive contribution to p_d^{elst} . The characteristic feature of configuration (c) is the formation of a hydrogen bond $\text{N}-\text{H}\cdots\text{O}$ between the ammonium and phosphate group. The attractive configurations coexisted with repulsive ones [such as in Fig. 6(a)], with the net result that p_d^{elst} proved to vanish. At this separation, the dominant pressure component was p_h , although p_d^{disp} and p_d^{rep} were almost equally significant. Note that the occurrence of an attractive interaction between the phosphate group in one membrane and the ammonium group in the opposing membrane has been assumed by McIntosh and Simon³² in an attempt to explain the much smaller equilibrium intermembrane spacing and maximum hydration of PEs as compared to the respective PCs. The simulations show, however, that such an attraction may indeed exist only at very short separations and it vanishes as the separation is increased. To gain more confidence in this conclusion, we undertook two short GCMC runs at $h=44.1$ and 45.6 Å starting from the final configuration of the system at $h=42.6$ Å. The difference in thickness was initially compensated by inserting an empty space in the center of the water layer. After 10^6 GCMC passes, the electrostatic attraction fell off and p_d^{elst} rose to 2–3 kbar.

B. Hydration degree

A disappointing result of the simulations is a too high hydration degree of the membranes. At the largest separation tried, $h=45.6$ Å, the hydration degree $n_w = \langle N \rangle / 64 = 13.1$, which even exceeds the experiment-based estimate of maximum hydration, $n_w^0 = 8.8\text{--}10.2$.^{11,30} A consequence of the overestimated hydration is a shift of the region of strong repulsion to larger h . At $h=45.6$ Å, the water-mediated pressure is still of the order of several kilobars (Table II), whereas the experimental pressure at the respective D (~ 47 Å) should be close to zero.^{11,30}

The too high hydration predicted by the simulations clearly points to a deficiency of the force field used, namely, to exaggerated hydrophilicity of the membranes due to an overestimated strength of the water-lipid interactions relative to the water-water and lipid-lipid ones. The water affinity of the DLPE membranes can be appreciated from Fig. 7, which shows the profile of the average interaction energy of a water molecule, $u(z)$, with all its surroundings as a function of the separation of the molecule from the midplane of the system. Also shown are the contributions to $u(z)$ from the water-water and water-lipid interactions. The horizontal dot-and-dash line at -19.8 kcal mole⁻¹ indicates, as a reference, the average interaction energy of a water molecule with its surrounding water molecules in bulk water at 308 K. It can be seen that the residence of a water molecule in the hydrophilic

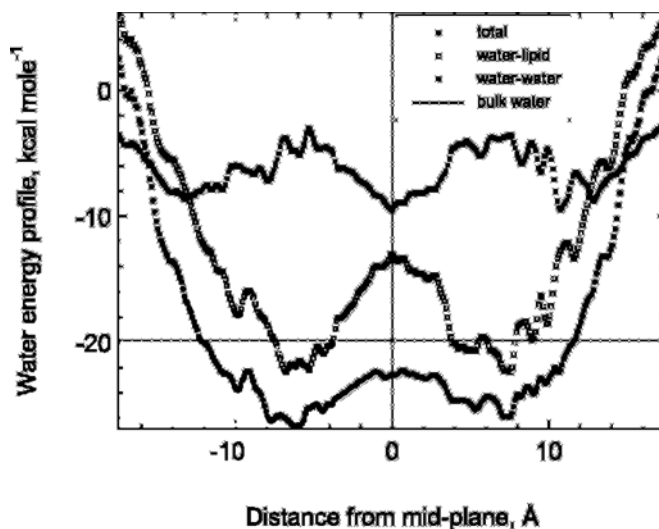


FIG. 7. Profiles of the average interaction energy of a water molecule with its surroundings.

region of the membranes is up to 7 kcal mole⁻¹ more favorable in energy compared to the water bulk. Even in the vicinity of the mid-plane, the water-lipid contribution to $u(z)$, which here comes mainly from protruded headgroups, is noticeably greater in magnitude than the water-water contribution.

C. Effect of methylation

In view of the property of the force field to exaggerate the hydrophilicity of DLPE, it was of interest to see whether the force field is capable of describing, at least qualitatively, the effect of full methylation of the terminal $-\text{NH}_3^+$ groups on hydration (i.e., the effect of going from DLPE to DLPC). In the AMBER-based force field,¹⁵ the methyls of the $-\text{N}(\text{CH}_3)_3^+$ group are treated in the united-atom approximation, so that the whole group is represented by a total of four force sites placed at the four nonhydrogen atoms. In this approximation, the $-\text{N}(\text{CH}_3)_3^+$ group differs from the $-\text{NH}_3^+$ one only in two respects: (1) the $\text{N}-\text{C}$ bond is by half longer than the $\text{N}-\text{H}$ one and (2) each united CH_3 atom of the former group bears both an electric charge (0.4 e) and a van der Waals force site, whereas each H atom of the latter group bears the same charge but no van der Waals force site. As a consequence, the $-\text{NH}_3^+$ group is capable of forming hydrogen bonds with water molecules, while $-\text{N}(\text{CH}_3)_3^+$ group is not. This difference can be appreciated from Fig. 8, which compares the distribution of water density around N atoms for both groups. For the $-\text{NH}_3^+$ group, the main maximum of the water density occurs at a $\text{O}\cdots\text{N}$ distance of ~ 2.8 Å, which is typical of the $\text{N}-\text{H}\cdots\text{O}$ hydrogen bond.

Considering the lower hydrophilicity of the $-\text{N}(\text{CH}_3)_3^+$ group, it may appear strange that DLPC shows a much higher maximum hydration, $n_w^0 \approx 35$,³³ compared to DLPE. Indeed, the common experience in studies of water confined between solid surfaces shows that the stronger the surface-liquid binding energy, the higher the average density of con-

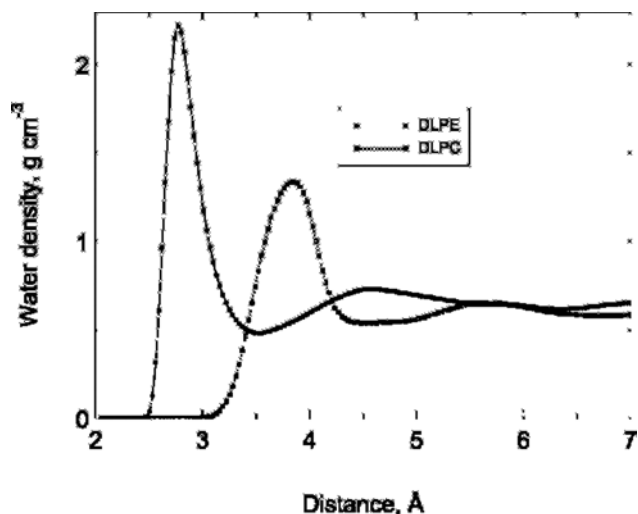


FIG. 8. Water density distribution around N atoms in hydrated DLPE and DLPC membranes.

finer liquid and the stronger the solvation (hydration) repulsion.³⁴ To clear up this point, we first studied the methylation effect in the “pure” form, namely, we just replaced the $-\text{NH}_3^+$ groups by the $-\text{N}(\text{CH}_3)_3^+$ ones while leaving the geometrical parameters of the system (A and h) unchanged. At $h=44.1$ Å, the result was a decrease in n_w from 11.7 to 9.4 Å, i.e., the methylated membranes imbibed substantially less water. In the next step, we increased A to its experimental value for DLPC ($A=68.7$ Å², i.e., noticeably higher than that of DLPE) and repeated the simulation. The final n_w was 19, i.e., much larger than the respective simulation result for DLPE (11.7). This provides a reasonable explanation for the much higher hydration degree of DLPC: Despite the lower hydrophilicity, DLPC membranes imbibe more water because of their lower areal density and, as a consequence, higher permeability. The latter fact can be appreciated from Fig. 9, which compares the water density profiles in DLPE and DLPC membranes. In the central part of the density

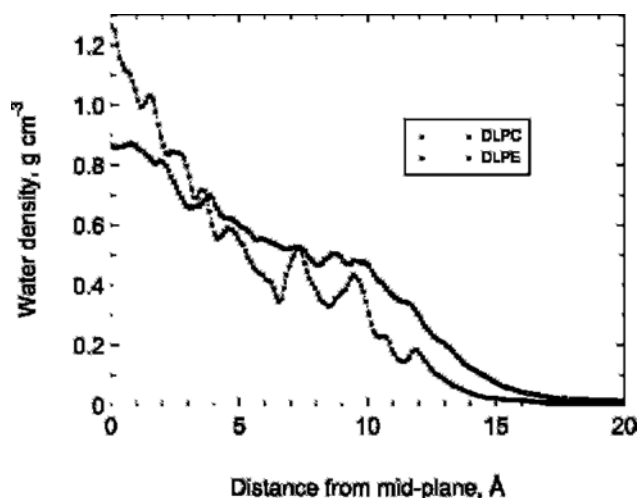


FIG. 9. Symmetrized water density profile for hydrated DLPE and DLPC membranes at $h=44.1$ Å.

distributions (0–5 Å from the midplane), the DLPC membranes show a lower water density because of the lower water affinity of the terminal $-\text{N}(\text{CH}_3)_3^+$ groups. However, on going toward the substrate, the water uptake by DLPC becomes higher than that of DLPE because DLPC provides more free space to accommodate water molecules.

Unlike the case of DLPE membranes, where the available literature data on A , D , and n_w are restricted to their values at full hydration,^{11,30} the structural parameters of DLPC membranes are known in a wide range of hydrations due to the x-ray diffraction study by Lis *et al.*³³ In comparing the experimental and simulation results, it should, however, be taken into account that our simulation and the measurements by Lis *et al.*³³ refer to different experimental conditions. The simulation mimics a SFA experiment, where the hydrated bilayers are compressed normally and the area per lipid A remains practically the same as that of the initially deposited bilayers. By contrast, the conditions of the experiments by Lis *et al.*³³ were equivalent to conditions of uniform hydrostatic compression, so that A noticeably decreased with decreasing n_w and D . The only reasonable comparison of the simulated and experimental systems is thus at similar values of A and D . Of the two values of A tried in our simulations ($A=52.1$ and 68.7 Å²), the former corresponds to a laterally compressed membrane and is more suitable for comparison. At $h=44.1$ Å, which roughly corresponds to $D\approx 45.5$ Å, the simulation resulted in $n_w=9.4$. The closest experimental values for A and D are³³ 55 Å and 45 Å², respectively, and the corresponding $n_w=6.2$. That is the simulated hydration is again too high compared to the experimental value.

D. Simulations with damped water-lipid interactions

The discrepancy between the experimental and simulated hydrations is hardly surprising in view of the fact that the force field used, as well as other force fields accepted in simulations of hydrated lipid membranes,³⁵ have never been tested for their ability to reproduce n_w in simulations of open systems, wherein water imbibed between the membranes is allowed to exchange particles with a bulk water reservoir.³⁶ In most cases, the simulations were carried out using the NVT ensemble MD, with n_w , D , and A fixed at the respective experimental values. The experimental hydration level was also adopted in NPT ensemble simulations, where D and A were allowed to fluctuate so as to keep P close to atmospheric pressure. The use of the NPT ensemble did ensure the mechanical equilibrium for hydrated membranes but did not ensure the chemical equilibrium between the confined and bulk water.

As far as the interfacial properties of water are concerned, the weakest point of the available united-atom force fields is, in our view, the parametrization of mixed (water-solute) interactions. In most cases, use is made of simple geometric and arithmetic-mean combining rules for parameters describing the interaction of force sites in dissimilar molecules. These rules are applied to both Coulombic and Lennard-Jones potentials. In the former case, the geometric-mean combining rule means that the interaction between sites i and

j in dissimilar molecules I and J is calculated with the same partial charges q_i and q_j as used in describing the interactions of homomolecular pairs $I \cdots I$ and $J \cdots J$. This rule would be strictly correct if q_i and q_j would be the actual physical charges on sites i and j . In fact, q_i and q_j are certain *effective* charges, which do not have a definite physical meaning and whose magnitudes strongly depend on the derivation method used.³⁷ In the particular force field¹⁵ used in our simulations, the charges on the lipid molecules were derived from *ab initio* SCF 6-31G* level electron density by Mulliken population analysis.³⁸ By contrast, the magnitudes and positions of the charges on the water molecule were derived, together with the Lennard-Jones parameters of the water oxygen, so as to reproduce the experimental energy and density of water at ambient conditions. It would be surprising if the effective charges derived in so different ways could well describe the electrostatic water-lipid interactions. The situation with Lennard-Jones potential parameters is similar.

To appreciate the effect of the water-lipid interaction strength on the hydration level and water-mediated pressure, we undertook a series of GCMC simulations with damped water-lipid interactions. The basic results for $\alpha=0.9$, 0.8, and 0.7 are presented in Table II. It can be seen that the damping of water-lipid interactions has a profound effect on the hydration level and pressure. Even a fairly small 10% damping ($\alpha=0.9$) reduces n_w by two water molecules per lipid and weakens the intermembrane repulsion by a factor of 2.6. In addition, the local water density at the midplane, which was as high as 1.25 g cm⁻³ at $\alpha=1$ (Fig. 2), reduces, at $\alpha=0.9$, to about 1 g cm⁻³. At a 20% damping ($\alpha=0.8$), one more molecule per lipid is lost and the repulsion drops by an order of magnitude, as compared to the initial force field. What is particularly interesting is the observed change in the mechanism of the water-mediated repulsion. Now the repulsion arises from the hydration component, whereas the net direct interaction between the membranes is attractive. The electrostatic component p_d^{elst} also changes its sign and becomes attractive, as is typical of electrically neutral surfaces bearing laterally and orientationally mobile polar groups. The reason is the partial dehydration of the opposing headgroups, which increases their mobility and allows them to assume energetically more favorable configurations. An analysis of the structural changes occurring in the system with decreasing α showed a reduction in the proportion of extended (unfolded) conformations of the headgroups. This change manifests itself in Fig. 4 as a noticeable drop in the occurrence of large N \cdots C₂ distances. In addition, the proportion of headgroups directed preferentially towards the opposing membrane decreased: The respective orientation parameter $S_{0,8}^{\text{PN}}$ fell from 0.8 to 0.6.

The change in the direct electrostatic intermembrane interaction from repulsion to attraction led to a substantial increase in the magnitude of the dispersion attraction p_d^{disp} and exchange repulsion p_d^{rep} . The reason is clear: With the initial force field ($\alpha=1$), the direct electrostatic repulsion of the membranes was longer ranged and it did not allow the opposing headgroups to approach close together. The change of

the electrostatic repulsion to attraction allowed closer contacts of the headgroups, thus leading to an increase in the magnitude of p_d^{disp} and p_d^{rep} .

Further damping of the water-lipid interactions ($\alpha=0.7$) made the DLPE membranes hydrophobic, in the sense that the total water-mediated pressure became attractive (Table II). The major factor responsible for the observed attraction was a strong attractive electrostatic component p_d^{elst} associated with lipid configurations similar to those in Figs. 6(b) and 6(c).

IV. CONCLUSIONS

Our GCMC simulations of hydrated DLPE membranes using a united-atom AMBER-based force field have revealed a mechanism that may in principle be responsible for the short-range intermembrane repulsion. In this mechanism, the water-mediated repulsion originates from the direct electrostatic interaction of PE headgroups protruded towards each other from the opposing membranes. The driving force behind the headgroup protrusions is a strong water affinity of the headgroups, which favors headgroup unfolding and reorientation. That is the origin of the protrusions has to do rather with the energetic than entropic factor, as in the model suggested by Israelachvili and Wennerström.^{2,7} The relevance of this mechanism to real intermembrane repulsion is, however, unclear because the force field used fails to reproduce the hydration degree of the membranes. The simulations of the hydrated membranes with damped water-lipid interaction potentials have shown that the hydration level and water-mediated pressure are very sensitive to the strength of the water-lipid interactions. Moreover, the damping of these interactions by only 10%–20% changes qualitatively the role of the individual pressure components in the intermembrane repulsion. It is also found that the water-lipid interactions and the direct intermembrane interactions are involved in a complicated interplay through the effect of the former on the conformational distribution of lipid headgroups. All these findings calls for the development of a force field designed specially for simulation of biointerphases, with emphasis placed on an adequate description of the balance between the homo- and heteromolecular pair interactions and between the intra- and intermolecular contributions to the potential energy of the system. It is attractive, in particular, to try polarizable force fields for water and biomolecular systems,³⁹ although the increased computational costs of such force fields over the fixed-charge models will hardly allow routine GCMC simulations of hydrated lipid membranes. Anyway, GCMC simulations can provide a stringent test for such force fields through a comparison of the experimental and simulated hydration levels.

Unlike theoretical treatments of the operative forces between neutral phospholipid membranes, where the direct electrostatic membrane-membrane interaction is usually ignored, the GCMC simulations reported in this article reveal a great importance of this kind of interaction, as represented by p_d^{elst} . Aside from a large relative magnitude of p_d^{elst} (see Table II), it depends in a complicated way on hydration,

membrane density, and intermembrane separation, thus being a controlling factor in the water-mediated interaction between the membranes.

- ¹R. Lipowsky and E. Sackmann, *Structure and Dynamics of Membranes* (Elsevier, Amsterdam, 1995), Vol. 1.
- ²J. N. Israelachvili and H. Wennerström, *J. Phys. Chem.* **96**, 520 (1992).
- ³R. Evans and U. M. B. Marconi, *J. Chem. Phys.* **86**, 7138 (1987).
- ⁴I. Langmuir, *J. Chem. Phys.* **6**, 873 (1938).
- ⁵B. V. Derjaguin and N. V. Churaev, in *Fluid Interfacial Phenomena*, edited by C. A. Croxton (Wiley, Chichester, 1986), Chap. 15.
- ⁶E. S. A. Jordine, *J. Colloid Interface Sci.* **45**, 435 (1973).
- ⁷J. Israelachvili and H. Wennerström, *Nature (London)* **379**, 219 (1996).
- ⁸V. A. Parsegian and R. P. Rand, *Langmuir* **7**, 1299 (1991).
- ⁹A. Pertsin, D. Platonov, and M. Grunze, *J. Chem. Phys.* **122**, 244708 (2005).
- ¹⁰M. Elder, P. Hitchcock, and R. Mason, *Proc. R. Soc. London, Ser. A* **354**, 157 (1977).
- ¹¹J. F. Nagle and M. C. Wiener, *Biochim. Biophys. Acta* **942**, 1 (1988).
- ¹²Initially, we tried to simulate the interaction of gel-phase DLPE membranes at room temperature and $A=42 \text{ \AA}$. It turned out, however, that the force field used failed to reproduce the gel state of the membranes, resulting in a substantially disordered structure corresponding rather to the liquid-crystalline state.
- ¹³S.-J. Marrink and H. J. C. Berendsen, *J. Phys. Chem.* **98**, 4155 (1994).
- ¹⁴P. Jedlovsky and M. Mezei, *J. Chem. Phys.* **111**, 10770 (1999).
- ¹⁵A. M. Smondyrev and M. L. Berkowitz, *J. Comput. Chem.* **20**, 531 (1999).
- ¹⁶D. P. Tieleman, URL <http://moose.bio.ucalgary.ca/files/pope.itp>.
- ¹⁷W. L. Jorgensen and J. D. Madura, *Mol. Phys.* **56**, 1381 (1985).
- ¹⁸H. Hauser, I. Pascher, R. H. Pearson, and S. Sundell, *Biochim. Biophys. Acta* **650**, 21 (1981).
- ¹⁹W. D. Cornell, P. Cieplak, C. I. Bayly, I. R. Gould, K. M. Merz Jr., D. M. Ferguson, D. C. Spellmeyer, T. Fox, J. W. Caldwell, and P. A. Kollman, *J. Am. Chem. Soc.* **117**, 5179 (1995).
- ²⁰T. Darden, D. York, and L. Pedersen, *J. Chem. Phys.* **98**, 10089 (1993).
- ²¹R. M. Venable, B. R. Brooks, and R. W. Pastor, *J. Chem. Phys.* **112**, 4822 (2000).
- ²²W. Shinoda, N. Namiki, and S. Okazaki, *J. Chem. Phys.* **106**, 5731 (1994).
- ²³The use of a statistical ensemble with a fixed lateral area of the simulation cell and a fixed number of lipid molecules could, in principle, partially suppress fluctuations in the local areal density of the lipid, which could affect the membrane permeability. For a simulation cell containing 32 symmetrically independent lipid molecules per monolayer, as in our case, the use of a fixed membrane area ensemble should however have little effect on the fluctuations in the local areal density. This follows from the MD results reported by S. E. Feller and R. W. Pastor, [*J. Chem. Phys.* **111**, 1281 (2005)] who compared the probability distributions of single molecule areas in fixed- and variable-area ensembles for a hydrated lipid membrane with 36 independent molecules per monolayer in the simulation cell.
- ²⁴M. R. Stapleton and A. Panagiotopoulos, *J. Chem. Phys.* **92**, 1285 (1990).
- ²⁵M. Mezei, *Mol. Phys.* **40**, 901 (1980).
- ²⁶R. H. Swendsen and J.-S. Wang, *Phys. Rev. Lett.* **58**, 86 (1987).
- ²⁷A. J. Pertsin, J. Hahn, and H.-P. Grossmann, *J. Comput. Chem.* **15**, 1121 (1994).
- ²⁸A. Pertsin and M. Grunze, *J. Phys. Chem. B* **108**, 16533 (2004).
- ²⁹D. J. Adams, *Mol. Phys.* **28**, 1241 (1974).
- ³⁰T. J. McIntosh and S. A. Simon, *Biochemistry* **25**, 4948 (1986).
- ³¹Throughout the article, the atom numbering is as suggested by Sundaralingam [*Ann. N.Y. Acad. Sci.* **195**, 324 (1972)]. The two carbon atoms in parentheses belong to the glycerol residue.
- ³²T. J. McIntosh and S. A. Simon, *Langmuir* **12**, 1622 (1996).
- ³³L. J. Lis, M. McAlister, N. Fuller, R. P. Rand, and V. A. Parsegian, *Biophys. J.* **37**, 657 (1982).
- ³⁴We here imply a large separation range, where the oscillations of water density and hydration pressure can be neglected.
- ³⁵M. Schlenkerich, J. Brickmann, A. D. MacKerell, Jr., and M. Karplus, in *Biological Membranes: A Molecular Perspective from Computation and Experiment*, edited by K. M. Merz, Jr. and B. Roux (Birkhäuser, Boston, 1996).
- ³⁶The GCMC simulations by Jedlovsky and Mezey (see Ref. 14), cited in the beginning of the previous section, were carried out at a lamellar repeat period D much larger than D^0 . No attempt to reproduce the experimental value of n_w was undertaken.
- ³⁷A. J. Pertsin and A. I. Kitaigorodsky, *The Atom-Atom Potential Method* (Springer, Berlin, 1987).
- ³⁸S.-W. Chiu, M. Clark, V. Balaji, S. Subramaniam, H. L. Scott, and E. Jakobsson, *Biophys. J.* **69**, 1230 (1995).
- ³⁹W. L. Jorgensen and J. Tirado-Rives, *Proc. Natl. Acad. Sci. U.S.A.* **102**, 6665 (2005).